BROADBAND HYPERSPECTRAL PHASE RETRIEVAL FROM NOISY DATA

Vladimir Katkovnik, Igor Shevkunov, Karen Egiazarian

Tampere University, Tampere, Finland, e-mail: vladimir.katkovnik@tuni.fi

ABSTRACT

Hyperspectral (HS) imaging retrieves information from data obtained across a wide spectral range of spectral channels. The object to reconstruct is a 3D cube, where two coordinates are spatial and third one is spectral. We assume that this cube is complex-valued, i.e. characterized spatially-frequency varying amplitude and phase. The observations are squared magnitudes measured as intensities summarized over spectrum. The HS phase retrieval problem is formulated as a reconstruction of the HS complex-valued object cube from Gaussian noisy intensity observations. The derived iterative algorithm includes the original proximal spectral analysis operator and the sparsity modeling for complex-valued 3D cubes. The efficiency of the algorithm is confirmed by simulation tests.

Index Terms— Hyperspectral phase retrieval, spectrum analysis, Fourier transform spectrometry, proximal spectral operator.

1. INTRODUCTION

Hyperspectral (HS) imaging retrieves information from hundreds to thousands channels across broad spectral ranges. Conventionally, these images are two-dimensional (2D) stacked together in 3D cubes, where first two coordinates are spatial (x, y) and third one is spectral, which is usually represented by wavelength λ or by wavenumber $k = 2\pi/\lambda$.

In recent years, HS coherent diffractive imaging (HSCDI) demonstrates a strong progress in high-resolution microscopy. The crucial challenge is to acquire phase information from intensity fields. An interference between reference and object wavefronts registered in diffraction patterns is used conventionally to resolve this problem. The typical examples of such approaches can be seen in the spectrally resolved interferometry [1, 2], Fourier Transform Holography [3, 4] and HS Digital Holography [2, 5, 6].

In this paper, we consider a class of HSCDI without reference beams. Two light beams, basic and its shifted copy, go through the object of interest. Thus, two identical but mutually shifted broadband patterns of the object are superposed on sensor. This scenario typical for Fourier-Transform Spectrometry (FTS) [7] leads to phase retrieval problems, where a complex-valued 3D object is obtained from indirect intensity observations as solutions of an ill-posed inverse problem. This inverse imaging results in a serious amplification of all kind of disturbances appeared in a reconstructed hyperspectral object, in particular, due to measurement noise. Besides, because of high spectral resolution, an energy obtained by sensors is separated between many narrow wave bands and limited in each band.

For noise suppression, straightforward sliding sample means along the wavelength dimension are used routinely (e.g. [8]). These denoising algorithms are not efficient and often lead to oversmoothing of object images.

Advanced algorithms for denoising of complex-domain HS data are proposed recently in [9, 10] based on the adaptive SVD analysis of noisy complex-valued 3D cube data.

The contribution of this paper can be summarized as follows. The HS phase retrieval is formalized as an optimization problem for Gaussian noisy observations given as total energy over the broadband wavelength interval. The proposed iterative algorithm is derived from optimization of the Gaussian log-likelihood provided nonlocal patch-wise complex domain sparsity modeling. We propose an original proximal operator enabling the spectral analysis of observations. Simulation experiments demonstrate that the HS phase retrieval can be efficiently resolved in the considered setup without random phase coding of wavefronts typical for the conventional phase retrieval techniques.

2. PROBLEM FORMULATION

Let $U_o(x, y, k) \in \mathbb{C}^{n\times m}$ be a 2D slice of a complex-valued 3D HS cube of size $n \times m$ on (x, y) provided a fixed spectral component k, and $Q_K(x, y) = \{U_0(x, y, k),\, k \in K\}$, $Q_K \in \mathbb{C}^{n\times m\times l_K}$, be an object spectral cube with l_K spectral components. The total size of the cube is $n \times m \times l_K$.

The lines of $Q_K(x, y)$ contain l_K spectral components corresponding to coordinates (x, y). This is a HS model of the object U_0.

The squared magnitude (intensity) observations may be written as:

$$Y_t = \sum_{k\in K} |U_{t,k}|^2,\; U_{t,k} = A_{t,k}U_{o,k},\; t \in T. \qquad (1)$$

Thanks to Jane and Aatos Erkko Foundation, Finland, supporting this research.

Here and in what follows, we use the vectorized representation for slices $U_0(x,y,k)$, $U_{o,k} \in \mathbb{C}^N$, $N = nm$, and $A_{t,k} \in \mathbb{C}^{M\times N}$ are linear operators of image formation modeling by propagation of 2D object images from the object plane to the sensor plane.

Thus, $U_{t,k} = A_{t,k}U_{o,k} \in \mathbb{C}^M$ are the complex-valued signals which intensities are registered by the sensor as $Y_t \in \mathbb{R}^M_+$. The summation on k in (1) says that the measurements are the total intensity calculated over all spectral components $U_{t,k}$. The squared absolute value $|.|^2$ in (1) is element-wise for components of the vectors $U_{t,k}$.

For noisy intensity observations $Z_t = Y_t + \varepsilon_t$, $t \in T$, where $\varepsilon_t \tilde{} \mathcal{N}(0,\sigma)$.

The HS phase retrieval from noisy data is formulated as a reconstruction of the HS object cube $Q_K(x,y)$ from the intensity observations $Z_t, t \in T$.

Remind that in the conventional setups of phase retrieval, the object U_o is reconstructed from observations

$$Z_t = |A_t U_o|^2 + \varepsilon_t,\ t \in T, \tag{2}$$

where both an object and observations do not depend on spectra and the index t denotes different observations.

The multispectral phase retrieval is proposed recently in [11] as a reconstruction of the object U_o from spectral observations $Y_t = \sum_{k\in K} |A_{t,k}U_o|^2, t \in T$.

Note, that in this setup the object U_o is invariant in spectral domain what seriously differs it from the problem studied in this paper.

We restrict the class of the operator $A_{t,k}$ to the form appeared in Fourier Transform Spectrometry [12] with the measured intensities Y_t in the form :

$$Y_t = \sum_{k\in K} |A_{t,k}U_{o,k}|^2, \tag{3}$$

$$A_{t,k} = (1 + e^{-jkt})A_k, t \in T. \tag{4}$$

In $A_{t,k}U_{o,k}$, two identical but mutually phase shifted broadband copies of the object $U_{o,k}$ are superposed on the sensor plane: basic $A_kU_{o,k}$ and phase shifted $e^{-jkt}A_kU_{o,k}$.

3. ALGORITHM DEVELOPMENT

3.1. Approach

The following is assumed concerning a sampling on t and k in the above observation modeling, $K = 0,1,...,N/2-1$, $T = 0,1,...,N-1$, then

$$Y_t = 2\sum_{k\in K}(1+\cos(\frac{2\pi}{N}kt))|B_k|^2, t \in T, \tag{5}$$

where $B_k = A_kU_{o,k}$, N is a number of observations and the integer discrete frequency k covers the low frequency interval $\{0,1,...,N/2-1\}$.

The restriction of this frequency interval to the length $N/2$ follows from the periodicity on t of the observation function (5). Provided that $|B_k|^2 = 0$ for $k = N/2,...,N-1$, the observations $\{Y_t\}$ uniquely define the intensity spectrum $|B_k|^2 \in K$ (see [13]).

The criterion for the algorithm design is of the form

$$J = \frac{1}{\sigma^2}\sum_{t=0}^{N-1}||Z_t - 2\sum_{k=0}^{N/2-1}|B_k|^2(1+\cos(\frac{2\pi}{N}kt))||_2^2 + \tag{6}$$

$$\frac{1}{\gamma}\sum_{k=1}^{N/2-1}||B_k - A_kU_{o,k}||_2^2 + f_{reg}(\{U_{o,k}\}_1^{N/2-1}).$$

The first summand stays for the Gaussian minus log-likelihood. The last third summand is a penalty formalizing a non-local patch-wise complex-domain sparsity hypothesis for the object images $\{U_{o,k}\}_1^{N/2-1}$. The complex domain $B_k = A_kU_{o,k}$ (spectral wavefronts at the sensor plane) are splitting variables separating the observations J_t from the object images. The second summand in J penalizes residuals between B_k and $A_kU_{o,k}$.

The object reconstruction is obtained by minimizing J on $\{U_{o,k}\}_1^{N/2-1}$. Note, that this set of the object images starts from $k = 1$, the zero order DC $k = 0$ is dropped in this optimization as we are interested only in the higher order components of the spectrum without this zero frequency item.

The developed algorithm iterates $\min_{B_k} J$ on B_k provided given $\{U_{o,k}\}_1^{N/2-1}$ and $\min_{\{U_{o,k}\}} J$ provided given $\{B_k\}$. Minimization on B_k concerns the two first summands in (6). This minimization can be interpreted as the proximity operator explicitly separating the estimates of the spectra $\{|B_k|^2\}$ from each others, i.e. producing the spectral analysis. Minimization on $U_{o,k}$ concerns the last two summands in (6).

In this paper instead of formalizing the penalty $f_{reg}(\{U_{o,k}\}_1^{N/2-1})$ we use the specially designed high-quality complex domain filter. It is in line with recent tendency in inverse imaging to use efficient filters for regularization.

3.2. Minimization on B_l

For minimization $\min_{B_l} J$, we solve the equations $\partial J/\partial B_l^* = 0, l = 1,...,N/2-1$, what leads to the complex-valued equations:

$$[\frac{-4}{\sigma^2}\sum_{t=0}^{N-1}Z_t\cos(\frac{2\pi}{N}kt) + \frac{8N}{\sigma^2}|B_l|^2 + \frac{1}{\gamma}]B_l = \frac{1}{\gamma}A_lU_{o,l}. \tag{7}$$

In this derivation we use that

$$\frac{1}{N}\sum_{t=0}^{N-1}Y_t = 2\sum_{k=0}^{N/2-1}|B_k|^2 + 2|B_0|^2 \tag{8}$$

and, then, for noisy Z_t and large N:

$$\frac{1}{N}\sum_{t=0}^{N-1} Z_t \simeq 2\sum_{k=0}^{N/2-1} |B_k|^2 + 2|B_0|^2. \quad (9)$$

Inserting $B_l = |B_l|e^{j\varphi_{B_l}}$ in (7), we may conclude that

$$\varphi_{B_l} = \varphi_{A_l U_{o,l}}, \quad (10)$$

where $\varphi_{A_l U_{o,l}}$ is phase of $A_l U_{o,l}$, as the expression in the squared brackets in (7) is real-valued.

It follows, that the magnitude of B_l is defined as a non-negative solution of the cubic polynomial equation:

$$[\frac{-4}{\sigma^2}\sum_{t=0}^{N-1} Z_t \cos(\frac{2\pi}{N}kt) + \frac{8N}{\sigma^2}|B_l|^2 + \frac{1}{\gamma}]|B_l| - \frac{1}{\gamma}|A_l U_{o,l}| = 0. \quad (11)$$

There is no the second power in this equation and the free term is negative, then there is only one positive solution $|B_l|$ [14] computed by Cardano's formulas.

Note that, calculations in the formulas (7)-(11) are produced in the pixel-wise manner, i.e. for each pixel separately: amplitude for B_l is given by (11) and the phase by (10).

This solution of $\min_{B_l} J$ can be interpreted as the proximity operator with a compact notation, following to [11], [15], as:

$$B_l = prox_{f.\gamma}(A_l U_{o,l}), l = 1, .., N/2 - 1, \quad (12)$$

where f stays for the minus log-likelihood part of (6), and $\gamma > 0$ is a parameter in (6).

The calculation of the cosine transform in (7),(11) can be produced using FFT for the sampling interval $T = \{0, 1, ..., N-1\}$ as it is in the above formulas (Proposition 2, [13]) or for the symmetric sampling interval $T = \{-N/2, -N/2+1, ..., , N/2-1\}$ (Proposition 4, [13]). This symmetric sampling is often in applications.

The proximity solution $\{B_l\}$ resolves two problems. Firstly, complex domain spectral components B_l are extracted from the intensity observations. Thus, we produce the spectral analysis of the observed total intensities. Secondly, the noisy observations are filtered with the power controlled by the regularization parameter γ compromising the noisy observations Z_t and the predicted $A_l U_{o,l}$ at the sensor plane.

3.3. Regularization by sparsity based filters

A similarity of the HS slices $U(x, y, k)$ for nearby wavenumbers k follows from the fact that on many occasions $U(x, y, k)$ are slowly varying functions of k as it for instance for the phase delays due to propagation of hyperspectral light through an object of varying thickness. Then, the spectral lines of $Q_k(x, y)$ live in k-dimensional subspaces with $k \ll l_K$. Therefore, the concept of sparsity can be applied for modelling of this phenomena.

In many recent applications and researches, plug-and-play filters have been recognized as a powerful tools for priors and regularization of inverse problems (e.g. [16], [17]). This approach to sparsity modeling in spectral and spacial domains is exploited in this paper in two different modes: joint and separate filtering spectral slices of the object cube.

The following algorithm is developed specially for the joint processing of slices in a HS cube [9, 10]:

$$\{\hat{U}_{o,k}, k \in K\} = \mathcal{CCF}\{U_{o,k}, k \in K\}. \quad (13)$$

Complex domain Cube Filter ($\mathcal{CCF}$) processes the data of the cube $\{\hat{U}_{o,k}, k \in K\}$ jointly and provide the estimates $\{\hat{U}_{o,k}, k \in K\}$ for all k.

The $\mathcal{CCF}$ algorithm is based on SVD analysis of the HS cube. It identifies an optimal subspace for the HS image representation including both the dimension of the eigenspace and eigenimages in this space. The Complex-Domain Block-Matching 3D (CDBM3D) algorithm [18, 19] filters this small number of eigenimages. Going from the eigenimage space back to the original image space we obtain the reconstruction of the object cube $\{U_{o,k}, k \in K\}$. This $\mathcal{CCF}$ algorithm is a complex domain modification of the fast algorithms developed for real-valued HS observations in [20] and [21].

A sliding window version of $\mathcal{CCF}$ was developed for objects with discontinuous and fast varying spectral characteristics [10].

3.4. HS phase retrieval algorithm

The forward/backward propagations from object to sensor and from sensor to object planes are included in the HS Phase Retrieval (HS-PhR) algorithm:

1. Initialization: $U_{o,k}^{(0)}, k \in K$;
2. For $s = 1, 2, ..., max_{iter}$ do;
3. Forward propagation: $U_{t,k}^{(s)} = A_k U_{o,k}^{(s)}, k \in K$;
4. Proximity operation: $B_k^{(s)} = prox_{f.\gamma}(U_{t,k}^{(s)}), k \in K$;
5. Backward propagation: $U_{o,k}^{(s)} = A_k^{\#} B_k^{(s)}, k \in K$;
6. $\mathcal{CCF}: \{U_{o,k}^{(s+1)}, \ k \in K\} = \mathcal{CCF}\{U_{o,k}^{(s)}, k \in K\}$;
7. Return $U_{o,k}^{(max_{iter})}, k \in K$.

Here $A_k^{\#}$ is an approximation for inverse of A_k. The noisy observations Z_t and estimates of the spectral variables $U_{t,k}^{(s)}$ are inputs of the proximity operator defining the next iteration as $U_{t,k}^{(s+1)}$ according to (11)-(12). A number of iterations max_{iter} is fixed in our experiments.

4. NUMERICAL VALIDATION

Multiple numerical experiments are produced with the HS-PhR algorithm for various HS objects and algorithm's parameters. We show here some of those results. It is assumed that

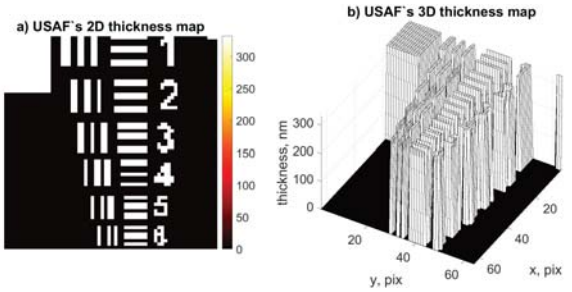

Fig. 1. Thickness of the transparent phase object: 2D (a) and 3D (b) images.

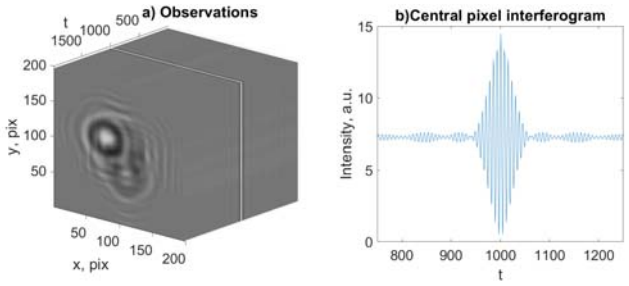

Fig. 3. (a) 3D noisy intensity observations: diffractive data cube Z_t; (b) The intensity distribution for the central pixel of the 3D data cube Z_t as a function of the slice number t.

the object is transparent with an invariant amplitude and a phase varying according to USAF test-image (see Fig.1). The parameters of these simulation tests correspond to some our physical experiments.

A broadband diode-laser light beam $\Lambda = [450 : 900]$ nm goes through the object and forms a 3D HS cube of intensity observations of the length $l_K = 2000$. The image formation wavelength dependent operators $A_{t,k}$ are calculated according to the angular spectrum wavefront propagation technique [22]. The proximity HS analysis is produced for 250 wavelengths ($N = 250$) and only 50 of them of higher signal-to-noise ratio are used for the phase retrieval iterations. We reconstruct the HS phase object of size $60 \times 60 \times 50$. The accuracy of the phase reconstruction is characterized by the relative root-mean-square-error (RRMSE) criterion:

$$\text{RRMSE} = \frac{\sqrt{||\hat{\varphi}_{est} - \varphi_{true}||_2^2}}{\sqrt{||\varphi_{true}||_2^2}}, \qquad (14)$$

where $\hat{\varphi}_{est}$ and φ_{true} are the reconstructed and true phases, respectively. RRMSE values less than 0.1 correspond to visually high quality $2D$ imaging.

The object thickness estimate obtained from the phase reconstruction for $\lambda = 730$ nm is presented in Fig.2 as $2D$ and $3D$ images which are nearly perfectly correspond to the true thickness images in Fig.1. The low value of RRMSE confirms the high-accuracy performance of the algorithm.

Fig.3 provides illustrations of the data used for object reconstruction. The fast convergence rate of the algorithm is demonstrated in Fig.4 as RRMSE values depending on iteration number s and on wavelength of the reconstructed slice of the object 3D cube. These results are obtained for noisy observations with $\sigma = .01$. The computational time is 350 sec/iteration for MATLAB R2019b on a computer with 32 GB of RAM and CPU with 3.40 GHz Intel (R) Core(TM) i7-3770 processor.

More simulation tests as well as results of physical experiments can be seen in [23].

5. CONCLUSION

A novel class of the HS phase retrieval problems is presented. The developed iterative algorithm uses the proximity spectral analysis operator and the HS sparsity modeling for complex-valued 3D cubes.

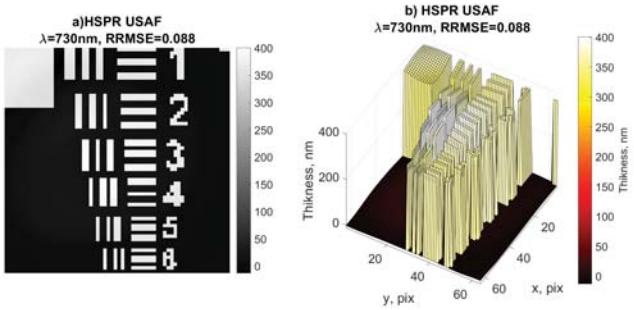

Fig. 2. Reconstruction of the object thickness obtained from the phase retrieval for the wavelength $\lambda = 730$ nm.

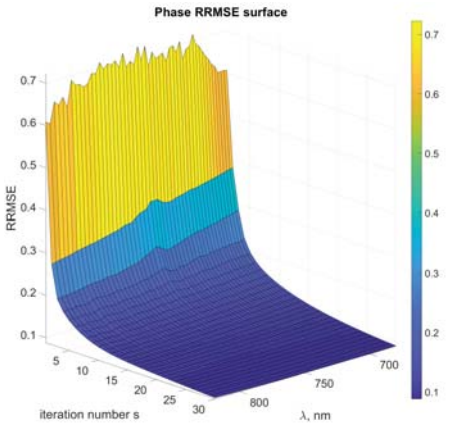

Fig. 4. RRMSE of the object phase reconstruction depending on iteration number s and wavelength λ.

6. REFERENCES

[1] Christophe Dorrer, Nadia Belabas, Jean-Pierre Likforman, and Manuel Joffre, "Spectral resolution and sampling issues in fourier-transform spectral interferometry," *JOSA B*, vol. 17, no. 10, pp. 1795–1802, 2000.

[2] SG Kalenkov, GS Kalenkov, and AE Shtanko, "Spectrally-spatial fourier-holography," *Optics express*, vol. 21, no. 21, pp. 24985–24990, 2013.

[3] Vasco T Tenner, Kjeld SE Eikema, and Stefan Witte, "Fourier transform holography with extended references using a coherent ultra-broadband light source," *Optics express*, vol. 22, no. 21, pp. 25397–25409, 2014.

[4] S Eisebitt, J Lüning, WF Schlotter, M Lörgen, O Hellwig, W Eberhardt, and J Stöhr, "Lensless imaging of magnetic nanostructures by x-ray spectro-holography," *Nature*, vol. 432, no. 7019, pp. 885, 2004.

[5] Dinesh N. Naik, Giancarlo Pedrini, Mitsuo Takeda, and Wolfgang Osten, "Spectrally resolved incoherent holography: 3D spatial and spectral imaging using a Mach–Zehnder radial-shearing interferometer," *Opt. Lett.*, vol. 39, no. 7, pp. 1857, apr 2014.

[6] D. Claus, G. Pedrini, D. Buchta, and W. Osten, "Accuracy enhanced and synthetic wavelength adjustable optical metrology via spectrally resolved digital holography," *Journal of the Optical Society of America A: Optics and Image Science, and Vision*, vol. 35, no. 4, pp. 546–552, 2018.

[7] Robert John Bell, *Introductory Fourier transform spectroscopy.*, Academic Press, 1972.

[8] S. G. Kalenkov, G. S. Kalenkov, and A. E. Shtanko, "Hyperspectral holography: an alternative application of the Fourier transform spectrometer," *Journal of the Optical Society of America B*, vol. 34, no. 5, pp. B49, 2017.

[9] Vladimir Katkovnik, Igor Shevkunov, Daniel Claus, Giancarlo Pedrini, and Karen Egiazarian, "Complex-domain joint broadband hyperspectral image denoising," *Sensors & Transducers*, vol. 233, no. 5, pp. 33–39, 2019.

[10] Igor Shevkunov, Vladimir Katkovnik, Daniel Claus, Giancarlo Pedrini, Nikolay Petrov, and Karen Egiazarian, "Hyperspectral phase imaging based on denoising in complex-valued eigensubspace," *Optics and Lasers in Engineering*, vol. 127, pp. 105973, 2020.

[11] Biel Roig-Solvas, Lee Makowski, and Dana H Brooks, "A proximal operator for multispectral phase retrieval problems," *SIAM Journal on Optimization*, vol. 29, no. 4, pp. 2594–2607, 2019.

[12] Robert Bell, *Introductory Fourier transform spectroscopy*, Elsevier, 2012.

[13] Vladimir Katkovnik, Igor Shevkunov, and Karen Egiazarian, "Hyperspectral holography and spectroscopy: computational features of inverse discrete cosine transform," *arXiv preprint arXiv:1910.03013*, 2019.

[14] Ferréol Soulez, Éric Thiébaut, Antony Schutz, André Ferrari, Frédéric Courbin, and Michael Unser, "Proximity operators for phase retrieval," *Applied optics*, vol. 55, no. 26, pp. 7412–7421, 2016.

[15] Neal Parikh, Stephen Boyd, et al., "Proximal algorithms," *Foundations and Trends® in Optimization*, vol. 1, no. 3, pp. 127–239, 2014.

[16] Singanallur V Venkatakrishnan, Charles A Bouman, and Brendt Wohlberg, "Plug-and-play priors for model based reconstruction," in *2013 IEEE Global Conference on Signal and Information Processing*. IEEE, 2013, pp. 945–948.

[17] Christopher A Metzler, Arian Maleki, and Richard G Baraniuk, "Bm3d-prgamp: Compressive phase retrieval based on bm3d denoising," in *2016 IEEE International Conference on Image Processing (ICIP)*. IEEE, 2016, pp. 2504–2508.

[18] Vladimir Katkovnik, Mykola Ponomarenko, and Karen Egiazarian, "Sparse approximations in complex domain based on BM3D modeling," *Signal Processing*, vol. 141, pp. 96–108, 12 2017.

[19] Vladimir Katkovnik and Karen Egiazarian, "Sparse phase imaging based on complex domain nonlocal BM3D techniques," *Digital Signal Processing: A Review Journal*, vol. 63, pp. 72–85, 4 2017.

[20] José M. Bioucas-Dias and José M.P. Nascimento, "Hyperspectral subspace identification," *IEEE Transactions on Geoscience and Remote Sensing*, vol. 46, no. 8, pp. 2435–2445, 2008.

[21] Lina Zhuang and Jose M. Bioucas-Dias, "Fast Hyperspectral Image Denoising and Inpainting Based on Low-Rank and Sparse Representations," *IEEE Journal of Selected Topics in Applied Earth Observations and Remote Sensing*, vol. 11, no. 3, pp. 730–742, 3 2018.

[22] Joseph W Goodman, *Introduction to Fourier optics*, Roberts and Company Publishers, 2005.

[23] Vladimir Katkovnik, Igor Shevkunov, and Karen Eguiazarian, "Hyperspectral phase retrieval," in *Unconventional Optical Imaging II*. International Society for Optics and Photonics, 2020, vol. 11351, pp. 127 – 136, SPIE.